Heliyon 8 (2022) e09218

Contents lists available at ScienceDirect

Heliyon

journal homepage: www.cell.com/heliyon

Research article

Biomechanical behaviour of PEDOT:PSS-based hydrogels as an electrode for stent integrated enzyme biofuel cells

Christina G. Antipova [a], Yulia M. Parunova [b], Maria V. Vishnevskaya [b], Sergey V. Krasheninnikov [a], Ksenia I. Lukanina [a], Timofei E. Grigoriev [a,c,*], Sergei N. Chvalun [a], Pavel M. Gotovtsev [b,c]

[a] National Research Centre "Kurchatov Institute", Department of Nanobiomaterials and Structures, Akademika Kurchatova pl., 1, 123182, Moscow, Russia
[b] National Research Centre "Kurchatov Institute", Biotechnology and Bioenergy Department, Akademika Kurchatova pl., 1, 123182, Moscow, Russia
[c] Moscow Institute of Physics and Technology (National Research University), 9 Institutskiy per., Dolgoprudny, Moscow Region, 141701, Russia

ARTICLE INFO

Keywords:
Biosensors
PEDOT:PSS
Biotechnology
Internet of things
Biofuel cell

ABSTRACT

The possibility of creating a biofuel cell based on a metal stent was shown in this study. Given the existing stent implantation approaches, the integration of a biofuel cell into a stent naturally entails capacity for biofuel cells to be installed into a human body. As a counter electrode, a hydrogel based on iota-carrageenan, polyvinyl alcohol, and PEDOT:PSS, with an immobilized glucose oxidase enzyme, was proposed. Tension tests demonstrated that the hydrogel mechanical behavior resembles that of a bovine's vein. To obtain an analytical description, the deformation curves were fitted using Gent and Ogden models, prompting the fitting parameters which can be useful in further investigations. During cyclic biaxial studies the samples strength was shown to decreases insignificantly in the first 50 cycles and, further, remains stable up to more than 100 cycles. The biofuel cell was designed with the PEDOT:PSS based material as an anode and a Co–Cr self-expanding stent as a cathode. The maximum biofuel cell power density with a glucose concentration of 5 mM was 7.87×10^{-5} W in phosphate buffer and 3.98×10^{-5} W in blood mimicking buffer. Thus, the biofuel cell integration in the self-expanding stent was demonstrated.

1. Introduction

Now, the active development of implantable medical devices is largely limited by the lack of permanent sources of power supply that can generate energy through the processes in the human body [1, 2]. Among many approaches to power generation, much attention is paid to biofuel cells (BFCs), which use various chemical substances as a substrate to generate energy. Glucose being an active participant in metabolism is presented in many physiological fluids and considered as the most promising BFC substrate [3, 4]. Nowadays, BFC are used to power various implantable devices. For example, in [5] BFC acted as an energy source for an animal brain stimulator, and in [6] it was used to supply ingestible device. Microelectronic sensors also can be supplied with energy from BFC [7]. The critical component of BFCs is electrodes. They should be made of materials that not only provide sorption of the enzyme acting as a catalyst, but also are biocompatible and have the required mechanical properties for interaction with physiological tissues and environments. The choice of materials also strongly affects the power properties of a BFC [3, 8, 9]. Besides, simple and effective implantation of a BFC is important as well.

Various types of materials for BFC electrodes are currently considered, including carbon nanomaterials [7, 10], systems with gold nanoparticles [11], modified textiles [12] and polymer hydrogels [13]. The latter are interesting because, depending on the selected polymers and the preparation technique, materials that mechanically behave almost the same as biological tissues can be obtained. Integration of an electrically conductive component into hydrogels provides use of such systems as electrodes for a BFC.

The most spread strategy for the electroconductive hydrogel synthesis is the inclusion of conductive polymers into a hydrogel [14]. Conductive polymers contain conjugated structures in backbone, which provide electrical conductivity due to the π bonds overlapping and creating of large chain segments where π-electrons are delocalized. Popular conjugated polymers, such as polyaniline, polypyrrole and polythiophene are extensively used in various applications since they show satisfying processability and high electrical conductivity [15, 16, 17]. Among others,

* Corresponding author.
E-mail address: timgrigo@gmail.com (T.E. Grigoriev).

https://doi.org/10.1016/j.heliyon.2022.e09218
Received 20 October 2021; Received in revised form 31 January 2022; Accepted 25 March 2022

polythiophene derivative, poly(3,4-ethylenedioxythiophene) (PEDOT), in a complex with poly(styrenesulfonate) (PSS) exhibits many valuable properties, in particular, water solubility, electrochemical and thermal stability, and relatively large conductivity – up to 900 S cm^{-1} [18]. Furthermore, PEDOT:PSS has adequate biocompatibility, which, combined with the other features, determines its usage in biomedical devices [19]. The polymer has been successfully used as an electrode component in BFC [20, 21]. In the present study, PEDOT:PSS provides conductivity of the materials.

The hydrogel component, in this study, is formed by two biocompatible polymers – polyvinyl alcohol (PVA) and iota-carrageenan (CRG). PVA is a non-toxic water-soluble synthetic polymer [22], whose chemical stability, acceptable mechanical and adhesive properties make it a strong candidate for electroconductive hydrogels production [23, 24] via physical cross-linking. Although different polymers, like polyacrylic acid or gelatin [13], can be used in such systems, PVA has been shown to exhibit good compatibility with PEDOT:PSS and even enhance conductive properties according to certain studies [25, 26]. Carrageenans are a family of high molecular weight sulfated polysaccharides extracted from red algae. This linear polymer consists of alternate units of D-galactose and 3, 6-anhydrogalactose, which are arbitrarily sulfated or non-sulfated. Subunits are connected by alpha 1–3 and beta 1-4-glycosidic bonds [27]. Due to its temperature-induced gelibility, excellent biocompatibility and bio-adequate mechanical properties, carrageenans are used for biotechnological applications, for example, biosensors, electrodes for biofuel cells [28, 29].

Implantation of electrodes into bloodstream can be a challenging task. Thus, the integration of a biofuel cell into a stent has the benefit of using stent implantation systems to install BFCs. Both arteries and veins are actively stented as a part of different cardiac illnesses treatment. In this study, we have concentrated on vein stenting systems as they are more convenient to use due to the lower pressure in the vessel, around 5 mmHg in large veins in comparison to 100 mmHg in arteries with the similar diameter [30, 31, 32, 33, 34].

The geometric configuration of a vessel flow channel is determined by its elastic-deformation state, or tone. The discrepancy between the mechanical behavior of the stent and the segment of the blood vessel can disrupt the structures of the blood flow boundary layer, change the velocity field and pressures in the lumen of the vessel, which inevitably lead to a rise in hydrodynamic resistance and increase risks of activating biologically active components of blood and the vascular wall, thrombus formation or hyperplasia [35, 36]. Ideally, the stent materials, in addition to the properties of thromboresistance and the ability to germinate should be biomechanically compatible to maintain adequate flow conditions and minimize perturbations in the blood flow [37, 38, 39]. The implantable electrode should as well be biomechanically suitable.

This article demonstrates the possibility of integration biopolymer-based electrodes into a stent for the vessel installation [40, 41]. The unification of a BFC and a stent creates an implantable electric generator, which, using already existing system of implantation, could be embedded into a human body.

2. Experimental section

2.1. Anode synthesis

The anode material is an electrically conductive biocompatible flexible hydrogel based on iota-carrageenan (Special Ingredients, Great Britain), polyvinyl alcohol 122000 g mol^{-1} (Avilon-Kompani Khim, Russia), and an electrically conductive polymer PEDOT:PSS (1.3 wt.% dispersion in H_2O, Sigma -Aldrich, USA) containing the glucose oxidase enzyme. The gel was prepared according to the technique presented earlier [42].

At the first stage two separate aqueous solutions of carrageenan and PVA with a concentration of 1.3 wt.% at the temperature 70 °C were made. Then equal amounts of the obtained solutions were mixed with a double amount of PEDOT:PSS aqueous suspension (1.3 wt.%). At the next stage, the resulting mixture was steered on a magnetic stirrer at the rate of 500–550 rpm and the temperature of 70 °C for 3 h. After cooling the reaction flask to room temperature, the mixture was processed by four sequent freezing/thawing cycles. During freezing, the sample was kept at the temperature of -12 °C, whereas during thawing – at room temperature. One cycle of freezing/thawing lasted for 24 h. At the last stage, the obtained samples were dried at 40 °C till constant weight. Glucose oxidase from *Aspergillus Niger* (Sigma Aldrich, USA) was added as a 10 mg ml^{-1} aqueous solution immediately prior to the sequential freeze/thawing step.

The size of the anode is approximately 5 × 15 mm.

2.2. Electron microscopy study

The morphology of the developed flexible electroconductive materials was investigated in a scanning electron microscope Versa 3D DualBeam (SEM, FEI, USA) in environmental scanning mode (ESEM). The SEM gaseous secondary electron detector was tuned on an accelerating voltage of 10 kV and a current of 60 pA. The samples were precooled to 3 °C on the Peltier stage before the experiment. For microstructural study the humidity in the vacuum chamber was consistently decreased from 100% to 60% during the experiment.

2.3. Mechanical properties study

Mechanical properties in uniaxial tension mode at a constant speed (1 mm min^{-1}) were studied using Instron 5965 universal testing machine (Illinois Tool Works Inc., USA) equipped with a ±50 N load sensor. The working part of the sample was 10.00 × 3.25 mm. The hydrogel preparation before testing includes swelling for two hours in physiological saline at 25 °C (this is enough to achieve equilibrium). A statistical sample were comprised of five vein specimens cut along the generatrix into 30 × 5 mm rectangles.

Also, the material was tested in puncture test and cyclic test (biaxial stress test). Thus, the strength of the hydrogel was estimated on surface stress.

In the mechanical tests we used the equipment which is similar to that used in testing film materials in ASTM D5748. As described in [43], "Performed at standard conditions, the test method imparts a biaxial stress that is representative of the type of stress encountered in many product end-use applications." ASTM D5748 assumes only a single loading of the test material until it fails. Since the primary interest was not to test the limiting characteristics but the stability of the mechanical behavior during long-term operation, we supplemented this type of test with multiple loading in the typical physiological load range. We used a scaled down version of the equipment described in ASTM D5748. The sample was fixed in a frame with a hole with a diameter of 8 mm. The indenter tip diameter was 3.5 mm. Preload was 0.02 N. The tests were carried out in the following modes: a single loading until the sample fracture and a cyclic loading (1000 cycles) in a physiological range of deformations and uniaxial tension.

2.4. Electrochemical study

The current-voltage characteristics (CVC) were measured on Autolab PGSTAT204 potentiostat-galvanostat (Metrohm, Switzerland) (NOVA 2.0 software) using a two-electrode circuit. The reference electrode was a saturated silver chloride $E = 0.222$ V. All measurements were carried out at room temperature (25 ± 1 °C) with a specified voltage from -300 to +300 and back to -300 mV (without interruption) with a potential sweep rate of 10 mVs^{-1} in a phosphate buffer solution (PBS), pH 7.4, with the addition of 0.15 M NaCl. No mediator was used in the experiments.

Different implantation conditions correlate with diverse physiological fluid compositions, including the content of fuel (substrate) and oxidant, as well as pH, and the presence of various components that can

influence the functioning of biological devices. Therefore, in order to simulate the conditions inside a blood vessel, electrochemical measurements were carried out in a solution that reproduces plasma composition, a blood mimicking buffer (BMB). One liter of the solution contains 5.9258 g NaCl, 0.3019 g KCl, 3.1643 g Na_2HPO_4*$2H_2O$, 0.6935 g NaH_2PO_4*H_2O, 0.05 mM ascorbate, 0.423 mM urate, 2.96 mM lactate, pH 7.39. The concentrations of ascorbate, lactate, and urate in the BMB were 0.058, 2.3, and 0.423 mM, respectively, which correspond to the average concentrations in human blood plasma [44, 45]. The measurements were carried out both in the absence of a substrate, glucose, and at a concentration of 5 mM. The substrate concentration of 5 mM corresponds to the normal glucose content in human blood plasma.

A Wallstant-Uni Endoprothesis self-expanding stent (Boston Scientific, USA) made of Co–Cr L605 alloy with a diameter of 6 mm was used as a cathode. To manufacture a biofuel cell, an electrically conductive Gox gel with a size of 5 × 20 mm was placed inside the stent; a hydrogel containing no electrically conductive components served as an interlayer between the stent and the electrically conductive gel. The entire system was immersed into the solution (PBS or BMB).

3. Results and discussion

3.1. Morphology study

Electron microscopy images showed in Figure 1b reveal classical gel film surface of PEDOT:PSS/PVA/CRG hydrogels. The surface has a smooth relief with the aggregates caused by cryogel formation procedure. Figure 1a shows that the presence of the carrageenan molecules leads to the appearance of folded elongated aggregates on the surface (and probably in volume) of the gels because of the double helices of iota-carrageenan, stabilized by K^+ ions during cryogel formation.

3.2. Mechanical study

The hydrogel was tested under uniaxial tension to calculate volume mechanical properties. A typical deformation curve (red) is shown in Figure 2a. Also, bovine jugular veins (Miratorg, Russia) were tested under the same conditions.

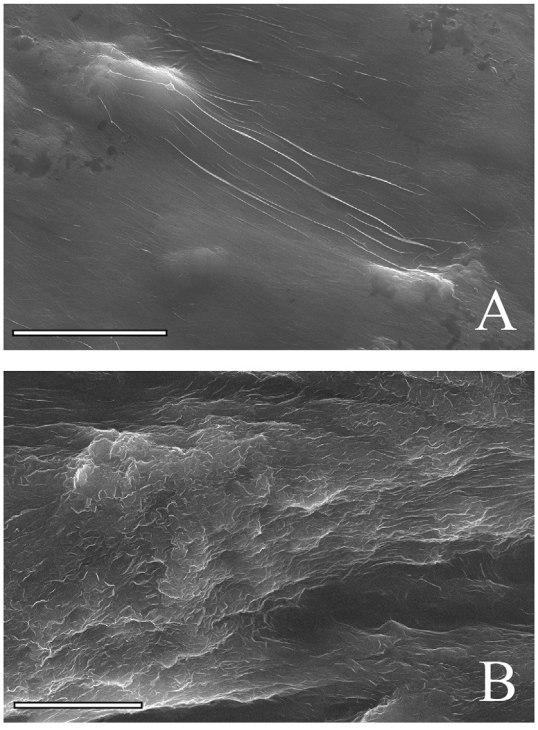

Figure 1. ESEM images of the hydrogel. (a) Folded elongated aggregates on the surface. (b) Classical hydrogelgel film surface. The scale bar is equal to 10 μm.

The hydrogel deformation curves have the characteristic shape for swollen polymers. The mechanical properties of the studied material were calculated: the elastic modulus – 42.2 ± 3.0 kPa, strength – 8.9 ± 0.9 kPa, and fracture strain – 20.8 ± 2.5 %

The result of hydrogel uniaxial tension tests is in a good agreement with mechanical behavior of vein under radial deformations. Figure 2a represents the first regions of the vein and the hydrogel deformation curves during uniaxial tension. They correlate well up to 20% strain (especially considering the fact that biological samples often have a range of results). Therefore, the hydrogel is likely to be non-traumatizing to ambient tissues. The observed mechanical properties of the sample are sufficient for the use, because the material is not expected to bear stress in the assumed application.

The numerical estimation of the curve parameters was made using different constitutive hyperelasticity models proposed by Arruda and Boyce, Haward, Gent, and Ogden. The last two models fit the experimental data best. Apparently, this is due to the fact that the first two models are based on the cross-links. In the proposed cryogel the cross-links include physical links formed by PVA crystalline areas as well as carrageenan double helices. The Gent and Ogden models, in turn, do not take into account molecular structure of the material. The approximation results are summarized in Table 1.

The Gent model [46] was originally introduced for the unfilled rubber vulcanizates as an empirical relation for the elastically stored energy density, W (Eq. (1)):

$$W = -\frac{E}{6} J_m \ln\left(1 - \frac{J_1}{J_m}\right) \tag{1}$$

where J_1 is the first invariant, defined as $J_1 = \lambda_1^2 + \lambda_2^2 + \lambda_3^2$, where $\lambda_1, \lambda_2, \lambda_3$ are the principle stretch ratios.

J_m is the maximum value of J_1, which corresponds to the fully stretched state of a network. $\frac{E}{3}$ is equal to μ, the shear modulus.

In case of uniaxial tension of incompressible material, the principle stretch ratios are $\lambda_1 = \lambda$, $\lambda_2 = \lambda_3 = \frac{1}{\sqrt{\lambda}}$. Using the obtained value for the J_m we can estimate the deformation at which the network is fully stretched. For the hydrogel the value is around 30%, and for the vein the value is 40%.

As well as the Gent model, the Ogden model [47] is a strain-energy function for isotropic incompressible rubbers. The relation is based on a linear combination of the strain invariants. The one-term Ogden model appears to be (Eq. (2)):

$$W = \frac{2\mu}{\alpha^2}\left(\lambda_1^\alpha + \lambda_2^\alpha + \lambda_3^\alpha - 3\right) \tag{2}$$

And for the uniaxial tension the stress-strain relation takes the form $\sigma = \frac{2\mu}{\alpha}\left(\lambda^{\alpha-1} - \lambda^{-\frac{\alpha}{2}-1}\right)$, where μ is the shear modulus, and α is a strain hardening exponent.

Both models (Eq. (1)) and (Eq. (2)) have been successfully applied for synthetic materials as well as for the native tissues [48, 49].

Mechanical puncture test were made to evaluate the strength characteristics of the developed materials. The Young's modulus of the sample was 63.3 kPa, and the strength was 10.2 kPa. A typical view of the deformation curve is shown in Figure 2b.

Thus, the strength properties of the 2:1:1 PEDOT:PSS/PVA/CGR hydrogel provides withstanding vessel pressure in excess. However, taking into account the pressure fluctuation in human body, the materials were tested under cyclic loads. The results are systematized in Table 2. Figure 2c shows typical curves for the 3rd and 997th loading cycle.

The analysis of the load amplitude during cyclic biaxial studies demonstrates that the samples strength insignificantly decreases in the first 50 cycles. Further, it is flattened and does not change until the end of the experiment as it is shown in Figure 2d. Apparently, this is caused by

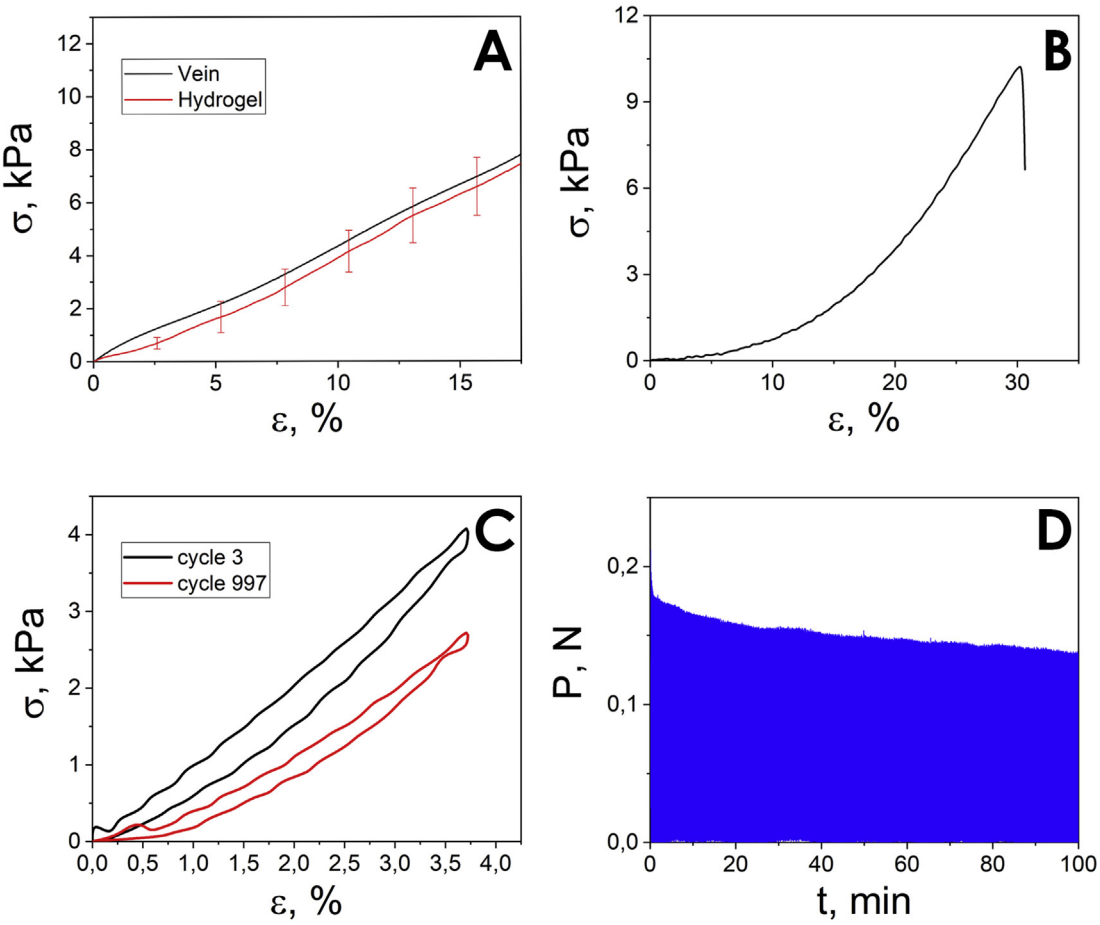

Figure 2. Typical deformation curves of the sample under (a) tension, (b) puncture, and cycle deformation (c) in 3rd and 997th cycles, (d) time scan.

the elimination of initial inhomogeneities in the sample. The hysteresis during the initial phase of the experiment also changes noticeably (decreases by more than a half), which indirectly confirms the aforementioned assumption. In addition, the analysis of the ratio of the hysteresis work to the total work of the deformation shows that after the 100th cycle this ratio is almost constant (the proportion of the hysteresis is 15–16%). This result indicates the mechanical stability of the studied sample.

The study of the composite mechanical behavior has revealed that the material strength properties correspond to those of the body soft tissues (tensile test). Biaxial studies have demonstrated a high biomechanical stability of the PEDOT:PSS/PVA/CGR composite material under the conditions close to the real organism. This is defined by the fact that each of the material components enhances the mechanical properties of the entire hydrogel. The proposed composite is a classic double network gel [50, 51], where each component contributes to the mechanical behavior of the hydrogel as a whole. The main gel-forming polymer is polyvinyl alcohol, which forms physical crosslinks during the freezing thawing process through the hydrogen bonds formation [52]. This network is responsible for increasing the overall elasticity modulus and also for strength characteristics. Carrageenan forms physical crosslinks by entanglements and aggregating helical regions [53, 54]. It is important that, in contrast to the polyvinyl alcohol crosslinks, the entanglements of carrageenan macromolecules are dynamic and labile. Such crosslinks, since they can be restored, enhance biomechanical stability under repeated cyclic loads. PEDOT is a rigid chain conjugated polymer, which also increases the elastic modulus of the hydrogel due to the greater rigidity of the elastically active chains.

3.3. Electrochemical study

A Wallstant-Uni Endoprothesis self-expanding stent (Boston Scientific) made of Co–Cr L605 alloy with a diameter of 6 mm was used as a cathode. The potential of the open circuit of the stent relative to the saturated silver chloride electrode in the first measurement was 0.297 V, then dropped to -0.003 V. In the second measurement, the potential dropped to -0.039 V. In the third measurement, carried out in both phosphate buffer and BMB, the same tendency to the negative direction shift was observed for OCP (up to -0.107 V in the first measurement cycle, -0.124 V in the second, and -0.138 V in the third). Such a shift negatively affects the power characteristics of the fuel cell and may be caused by

Table 1. Fitting results.

Sample	Model			
	Gent		Ogden	
	μ, kPa	J_m	μ, kPa	α
Hydrogel	14.5 ± 2.1	0.23 ± 0.09	13.3 ± 2.2	9.2 ± 1.9
Vein	16.2 ± 2.9	0.37 ± 0.07	14.6 ± 2.0	8.4 ± 1.6

Table 2. Cyclic test results.

Hysteresis area $\times 10^{-3}$ (3 цикл)	8.87 ± 0.04
Hysteresis area $\times 10^{-3}$ (997 цикл)	4.54 ± 0.10
Hysteresis area difference (3 and 997 cycles)	51.60 ± 1.70
Slope of the elastic region, N/mm	0.46 ± 0.07
Slope of the elastic region, MPa	0.21 ± 0.01
Estimated strength, kPa	8.80 ± 0.70

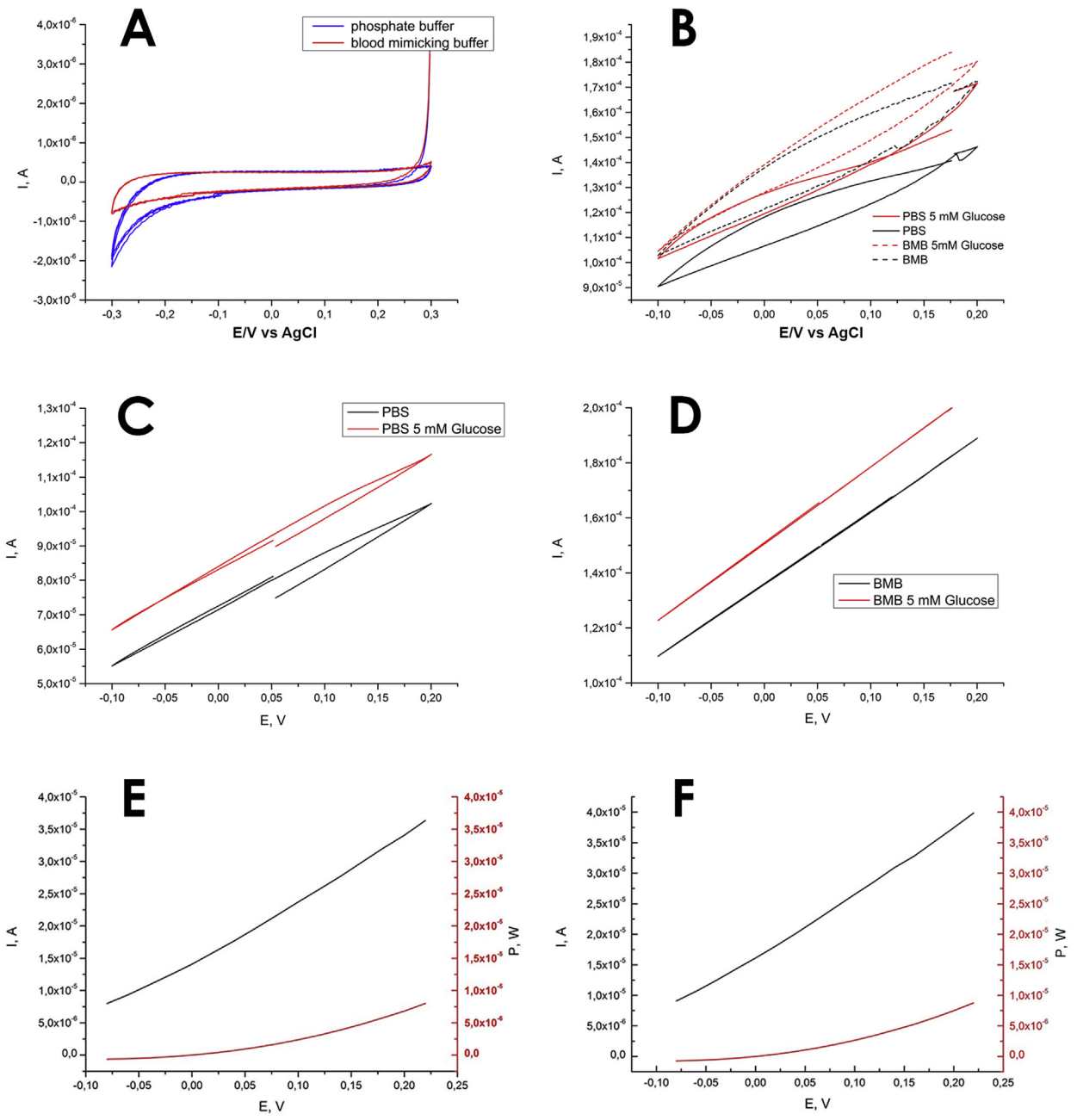

Figure 3. (a) Cathodic cyclic voltograms of the stents in PBS and BMB, sweep rate 10 mV s^{-1}; (b) Anodic cyclic voltograms of the hydrogel with Gox in PBS and BMB in the presence of 5 mM glucose and without it, sweep rate 10 mV s^{-1}. Cyclic voltograms of the biofuel cell, where the anode is the hydrogel with Gox and the cathode is the coronary stent, in (c) PBS and (d) BMB in the presence of 5 mM glucose and without it, the sweep rate is 10 mV s^{-1}. Polarization curves and power curves of the biofuel cell, where the anode is the hydrogel with Gox and the cathode is the coronary stent, in (e) PBS and (f) BMB in the presence of 5 mM glucose

electrochemical material behavior in the presence of electric current and pH changes in the near-surface layer.

Cathodic cyclic voltograms in PBS and BMB are shown in Figure 3a. Anodic cyclic voltograms in PBS and BMB are shown in Figure 3b. From the CV data of the anode in PBS and BMB in the presence of 5 mM glucose, a catalytic current of 2.6 μA and 0.8 μA, respectively, was observed (at an electrode potential of 0.2 V). Probably, a decrease in the catalytic current at the anode in BMB is associated with a decrease in the conductivity of the gel as a whole. This effect can be explained by the lesser swelling of gels based on CRG-PVA with an increase in the salt content of solutions and the effect of solution components on the gel structure [55].

Data presented in Figures 3c and 3d shows that the current in the BFC operating in the BMB reaches 2.4×10^{-4} A, which is slightly higher than that in the case of PBS. These figures also demonstrate that in the presence of glucose, the BFC generates larger currents. Figures 3e and 3f demonstrates polarization curves, which were used for the cell power calculation according to (Eq. (3)):

$$P = I \times U, \tag{3}$$

where P is power, I and U are current and voltage, respectively. The maximum cell power density with a glucose concentration of 5 mM was 7.99×10^{-6} W in PBS and 8.75×10^{-6} W in BMB.

It is worth noting that the cell power can be further increased using a stent made of more cathode suitable material.

4. Conclusion

In this study, we proposed a three-component electroconductive hydrogel containing polyvinyl alcohol, carrageenan and PEDOT:PSS for application as a BFC electrode integrated into a stent. This composite is a typical double network gel, which determines its mechanical stability. As the expected application of the hydrogel is the integration into the cardiovascular system, the mechanical behaviour of the material was compared to that of a vein. To obtain analytical parameters of the deformation curves, we selected constitutive models relevant for both vein and the hydrogel. The Gent and Ogden models fit the deformation curves best. Analysis of the hydrogel properties showed that it has the similar shear modulus to the vein one. Along with good cyclic stability this suggests the PEDOT:PSS-based material is sufficient for the stable operation under mechanical impacts typical for the blood flow. Electrochemical study demonstrated that such system can achieve power equal to 3.98×10^{-5} W. The further power increase is possible by means of the cathode part improvement, namely, modification of the stent material considering its operation as a BFC cathode. Thus, it is possible to create a biofuel cell integrated into a stent for vascular surgery, which allows the use of all stenting options for the installation of such power-generating devices. Future research will focus on the investigation of the proposed system under dynamic conditions with the imitation of implantation using existing solutions for the vascular stenting and real fluid flow.

Declarations

Author contribution statement

Christina G. Antipova, Yulia M. Parunova, Sergey V. Krasheninnikov: Conceived and designed the experiments; Performed the experiments; Analyzed and interpreted the data; Wrote the paper.

Maria V. Vishnevskaya: Conceived and designed the experiments; Performed the experiments.

Ksenia I. Lukanina: Conceived and designed the experiments; Analyzed and interpreted the data; Wrote the paper.

Timofei E. Grigoriev: Conceived and designed the experiments; Analyzed and interpreted the data; Contributed reagents, materials, analysis tools or data.

Sergei N. Chvalun: Conceived and designed the experiments; Analyzed and interpreted the data.

Pavel M. Gotovtsev: Conceived and designed the experiments; Performed the experiments; Analyzed and interpreted the data; Contributed reagents, materials, analysis tools or data; Wrote the paper.

Funding statement

This work was supported by Russian Foundation for Basic Research (RFBR) (18-29-23024mk).

Data availability statement

Data will be made available on request.

Declaration of interests statement

The authors declare no conflict of interest.

Additional information

No additional information is available for this paper.

Acknowledgements

The experiments were performed using the equipment of the Resource Center for Probe and Electron Microscopy (Kurchatov Complex of NBICS Nature-like Technologies, National Research Center Kurchatov Institute).

References

[1] M. Gamella, A. Koushanpour, E. Katz, Biofuel cells-activation of micro and macro-electronic devices, Bioelectrochemistry 119 (2018) 33–42.
[2] M. Rasmussen, S. Abdellaoui, S. Minteer, Enzymatic biofuel cells: 30 years of critical advancements, Biosens. Bioelectron. 15 (76) (2016) 91–102.
[3] S. Cosnier, A.L. Go, M. Holzinger, Towards glucose biofuel cells implanted in human body for powering artificial organs: Review, Electrochem. Commun. 38 (2014) 19–23.
[4] B. Rapoport, J. Kedzierski, R. Sarpeshkar, A glucose fuel cell for implantable brain-machine interfaces, PLoS One 7 (2012), e38436.
[5] D. Lee, S. Jeong, S. Yun, S. Kim, J. Sung, J. Seo, S. Son, J. Kim, L. Susanti, Y. Jeong, S. Park, K. Seo, S. Kim, T. Chung, Totally implantable enzymatic biofuel cell and brain stimulator operating in bird through wireless communication, Biosens. Bioelectron. 171 (2021) 112746.
[6] P. Nadeau, D. El-Damak, D. Glettig, Y. Kong, S. Mo, C. Cleveland, L. Booth, N. Roxhed, R. Langer, A. Chandrakasan, G. Traverso, Prolonged energy harvesting for ingestible devices, Nat. Biomed. Eng. 1. doi:.
[7] P. Bollella, I. Lee, D. Blaauw, E. Katz, A microelectronic sensor device powered by a small implantable biofuel cell, ChemPhysChem 21 (2020) 120–128.
[8] A. Zebda, S. Cosnier, J.-P. Alcaraz, M. Holzinger, A.L. Go, C. Gondran, F. Boucher, F. Giroud, K. Gorgy, H. Lamraoui, P. Cinquin, Single glucose biofuel cells implanted in rats power electronic devices, Sci. Rep. 3 (2013) 1516.
[9] A. Zebda, J. Alcaraz, P. Vadgama, S. Shleev, S. Minteer, F. Boucher, P. Cinquin, D. Martin, Challenges for successful implantation of biofuel cells, Bioelectrochemistry 124 (2018) 57–72.
[10] M. Islam, S. Arata, K. Hayashi, A. Kobayashi, Y. Momoi, K. Niitsu, Biomedical application via implantable devices by cmos-compatible glucose fuel cells using carbon nano horn, ECS Transac. 97 (2020) 311–319.
[11] V. Andoralov, M. Falk, D. Suyatin, M. Granmo, J. Sotres, R. Ludwig, V. Popov, J. Schouenborg, Z. Blum, S. Shleev, Biofuel cell based on microscale nanostructured electrodes with inductive coupling to rat brain neurons, Sci. Rep. 3 (2013) 1–11.
[12] J. Lv, I. Jeerapan, F. Tehrani, L. Yin, C. Silva-Lopez, J.-H. Jang, D. Joshuia, R. Shah, Y. Liang, L. Xie, F. Soto, C. Chen, E. Karshalev, C. Kong, Z. Yang, J. Wang, Sweat-based wearable energy harvesting storage hybrid textile devices, Energy Environ. Sci. 11 (2018) 3431–3442.
[13] H. Lu, N. Zhang, M. Ma, Electroconductive hydrogels for biomedical applications, WIREs Nanomed. Nanobiotech. 11 (2019) e1568.
[14] B.W. Walker, R.P. Lara, E. Mogadam, C.H. Yu, W. Kimball, N. Annabi, Rational design of microfabricated electroconductive hydrogels for biomedical applications, Prog. Polym. Sci. 92 (2019) 135–157.
[15] A. Taghizadeh, M. Taghizadeh, M. Jouyandeh, M.K. Yazdi, P. Zarrintaj, M.R. Saeb, E.C. Lima, V.K. Gupta, Conductive polymers in water treatment: a review, J. Mol. Liq. 312 (2020) 113447.
[16] Z. Qiu, B.A. Hammer, K. Mullen, Conjugated polymers - problems and promises, Prog. Polym. Sci. 100 (2020) 101179.
[17] M. Saadeh, P. Frere, B. Guiard, Revealing the flexoelectric-like response of poly(3,4-ethylenedioxythiophene):poly(styrenesulfonate) thin films, Poly. Adv. Technol. 31 (2020) 2632–2639.
[18] J. Gu, S. Gao, Y. Xue, J. Li, C. Wang, Q. Ren, G. Sheng, Synthesis and characterization of pedot aqueous dispersions with sulfonated polyfluorene as a template and doping agent, React. Funct. Polym. 100 (2016) 83–88.
[19] S. Panigrahy, B. Kandasubramanian, Polymeric thermoelectric PEDOT:PSS and composites: synthesis, progress, and applications, Eur. Polym. J. 132 (2020) 109726.
[20] J. R. B. Shetty, D. Ganapathy, P. Murugan, R. Atchudan, D. Umapathy, A. Khosla, A. Sundramoorthy, Thermally expanded graphite incorporated with PEDOT:PSS based anode for microbial fuel cells with high bioelectricity production, J. Electrochem. Soc.
[21] L. Yin, J.-M. Moon, J. Sempionatto, M. Lin, M. Cao, A. Trifonov, F. Zhang, Z. Lou, J.-M. Jeong, S.-J. Lee, S. Xu, J. Wang, A passive perspiration biofuel cell: high energy return on investment, Joule 5 (2021) 1888–1904.
[22] M. Teodorescu, M. Bercea, S. Morariu, Biomaterials of poly(vinyl alcohol) and natural polymers, Polym. Rev. 58 (2018) 247–287.
[23] M. Aslam, M.A. Kalyar, Z.A. Raza, Polyvinyl alcohol: a review of research status and use of polyvinyl alcohol based nanocomposites, Polym. Eng. Sci. 58 (12) (2018) 2119–2132.
[24] T. Gupta, A. Pradhan, S. Bandyopadhyay-Ghosh, S.B. Ghosh, Thermally exfoliated graphene oxide reinforced stress responsive conductive nanocomposite hydrogel, Poly. Adv. Technol. 30 (2019) 2392–2401.
[25] J.S. Hwang, T.H. Oh, S.H. Kim, S.S. Han, S.J. Lee, S.G. Lee, Y.J. Lee, S.S. Jang, Effect of solvent on electrical conductivity and gas sensitivity of PEDOT:PSS polymer composite films, J. Appl. Polym. Sci. 132 (2015) 42628.
[26] V. Mydhili, S. Manivannan, Effect of microstructure on the dielectric properties of poly(vinyl alcohol){poly(3,4-ethylenedioxythiophene) doped with poly(styrenesulfonate) composite films, J. Appl. Polym. Sci. 134 (2017) 45079.

[27] J.-L. Jiang, W.-Z. Zhang, W.-X. Ni, J.-W. Shao, Insight on structure property relationships of carrageenan from marine red algal: a review, Carbohydr. Polym. 257 (2021) 117642.
[28] J. Venkatesan, S. Anil, S.-K. Kim, Seaweed Polysaccharides. Isolation, Biological and Biomedical Applications, Elsivier, 2017.
[29] C. Esmaeili, M. Ghasemi, L. Heng, S. Hassan, M. Abdi, W. Daud, H. Ilbeygi, A. Ismail, Synthesis and application of polypyrrole/carrageenan nano-biocomposite as a cathode catalyst in microbial fuel cells, Carbohydr. Polym. 114 (2014) 253–259, 072.
[30] A. Jayaraj, W. Buck, A. Knight, B. Johns, S. Raju, Impact of degree of stenosis in may-thurner syndrome on iliac vein stenting, J. Vasc. Surg.: Venous Lymph. Disorders 7 (2019) 195.
[31] M.L. Montminy, J.D. Thomasson, G.J. Tanaka, L.M. Lamanilao, W. Crim, S. Raju, A comparison between intravascular ultrasound and venography in identifying key parameters essential for iliac vein stenting, J. Vasc. Surg.: Venous Lymph. Disorders 7 (2019) 801.
[32] A. S. Badesha, P. R. S. Bains, B. R. S. Bains, T. Khan, A systematic review and meta-analysis of the treatment of obstructive chronic deep venous disease using dedicated venous stents, J. Vasc. Surg.: Venous Lymph. Disorders.
[33] J.-H. Park, J.-H. Lee, Carotid artery stenting, Korean Circulat. J. 48 (2018) 97.
[34] D. Camasao, D. Mantovani, The mechanical characterization of blood vessels and their substitutes in the continuous quest for physiological-relevant performances. a critical review, Mater. Today Biol. 10 (2021) 100106.
[35] S. de Valence, J.-C. Tille, D. Mugnai, W. Mrowczynski, R. Gurny, M. Moller, B.H. Walpoth, Long term performance of polycaprolactone vascular grafts in a rat abdominal aorta replacement model, Biomaterials 33 (1) (2012) 38–47.
[36] V. Sottiurai, Distal anastomotic intimal hyperplasia: histocytomorphology, pathophysiology, etiology, and prevention, Int. J. Angiol. 8 (1) (1999) 1–10.
[37] S.E. Greenwald, C.L. Berry, Improving vascular grafts: the importance of mechanical and haemodynamic properties, Special Issue: modern Concepts in Vascular, Pathology 190 (3) (2000) 292–299.
[38] D.G. Simpson, G.L. Bowlin, Tissue-engineering scaffolds: can we reengineer mother nature? Expet Rev. Med. Dev. 3 (1) (2006) 9–15.
[39] M.W. Weston, K. Rhee, J.M. Tarbell, Compliance and diameter mismatch affect the wall shear rate distribution near an end-to-end anastomosis, J. Biomech. 29 (2) (1996) 187–198.
[40] R. Ahmed, M. Wilkinson, G. Parker, M. Thurtell, J. Macdonald, P. Mc-Cluskey, R. Allan, V. Dunne, M. Hanlon, B. Owler, G. Halmagyi, Transverse sinus stenting for idiopathic intracranial hypertension: a review of 52 patients and of model predictions, Am. J. Neuroradiol. 32 (2011) 1408–1414.
[41] A. Maskanakis, N. Patelis, D. Moris, D. Tsilimigras, D. Schizas, M. Diakomi, C. Bakoyiannis, S. Georgopoulos, C. Klonaris, T. Liakakos, Stenting of subclavian artery true and false aneurysms: a systematic review, Ann. Vasc. Surg. 47 (2018) 291–304.
[42] P. Gotovtsev, G. Badranova, Y. Zubavichus, N. Chumakov, C. Antipova, R. Kamyshinsky, M. Presniakov, K. Tokaev, T. Grigoriev, P.E.D.O.T. Electroconductive, PSS-based hydrogel prepared by freezing-thawing method, Heliyon 5 (9) (2019), e02498.
[43] Astm d5748-95(2019), Standard Test Method for Protrusion Puncture Resistance of Stretch Wrap Fulm, Tech. Rep., ASTM International, West Conshohocken, PA, 2019.
[44] J. Lykkesfeldt, Ascorbate and dehydroascorbic acid as reliable biomarkers of oxidative stress: analytical reproducibility and long-term stability of plasma samples subjected to acidic deproteinization, Canc. Epidemiol. Biomark. Prevent. 16 (11) (2007) 2513–2516.
[45] M. Wiecek, M. Maciejczyk, J. Szymura, Z. Szygula, Changes in oxidative stress and acid-base balance in men and women following maximal-intensity physical exercise, Canc. Epidemiol. Biomark. Prevent. 64 (1) (2015) 93–102.
[46] A.N. Gent, A new constitutive relation for rubber, Rubber Chem. Technol. 69 (1996) 59.
[47] R.W. Ogden, Large deformation isotropic elasticity - on the correlation of theory and experiment for incompressible rubberlike solids, Proc. Royal Soc. A 326 (1972) 565.
[48] O.A. Shergold, N.A. Fleck, D. Radford, The uniaxial stress versus strain response of pig skin and silicone rubber at low and high strain rates, Int. J. Impact Eng. 32 (2006) 1384.
[49] L.A. Mihail, L. Chin, P.A. Janmey, A. Goriely, A comparison of hyperelastic constitutive models applicable to brain and fat tissues, J. R. Soc. Interface 12 (2015) 20150486.
[50] X. Huang, J. Li, J. Luo, Q. Gao, A. Mao, J. Li, Research progress on doublenetwork hydrogels, Mater. Today Commun. 29 (2021) 102757.
[51] Q. Chen, H. Chen, L. Zhua, J. Zheng, Fundamentals of double network hydrogels, J. Mater. Chem. B 3 (2015) 3654.
[52] H. Adelnia, R. Ensandoost, S.S. Moonshi, J.N. Gavgani, E.I. Vasa, H.T. Ta, Freeze/thawed polyvinyl alcohol hydrogels: present, past and future, Eur. Polym. J. 164 (2022) 110974.
[53] C. Croitoru, M.A. Pop, T. Bedo, M. Cosnita, I.C. Roata, I. Hulka, Physically crosslinked poly (vinyl alcohol)/kappa-carrageenan hydrogels: structure and applications, Polymers 3 (2020) 560.
[54] S.J.L.P. Perez, G.C. Claudio, Molecular dynamics simulations of two double-helical hexamer fragments of iota-carrageenan in aqueous solution, J. Mol. Graph. Model. 98 (2020) 107588.
[55] G. Badranova, P. Gotovtsev, Y. Zubavichus, I. Staroselskiy, A. Vasiliev, I. Trunkin, M. Fedorov, Biopolymer-based hydrogels for encapsulation of photocatalytic TiO_2 nanoparticles prepared by the freezing/thawing method, J. Mol. Liq. 223 (2016) 16–20.